Nerve guides manufactured from photocurable polymers to aid peripheral nerve repair

Christopher J. Pateman [a], [1], Adam J. Harding [b], [1], Adam Glen [a], Caroline S. Taylor [a], Claire R. Christmas [b], Peter P. Robinson [b], Steve Rimmer [c], Fiona M. Boissonade [b], [**], Frederik Claeyssens [a], [***], John W. Haycock [a], [*]

[a] Department of Materials Science and Engineering, Kroto Research Institute, Broad Lane, University of Sheffield, Sheffield S3 7HQ, UK
[b] Integrated Biosciences Group, School of Clinical Dentistry, University of Sheffield, UK
[c] Department of Chemistry, University of Sheffield, Sheffield, UK

ARTICLE INFO

ABSTRACT

The peripheral nervous system has a limited innate capacity for self-repair following injury, and surgical intervention is often required. For injuries greater than a few millimeters autografting is standard practice although it is associated with donor site morbidity and is limited in its availability. Because of this, nerve guidance conduits (NGCs) can be viewed as an advantageous alternative, but currently have limited efficacy for short and large injury gaps in comparison to autograft. Current commercially available NGC designs rely on existing regulatory approved materials and traditional production methods, limiting improvement of their design. The aim of this study was to establish a novel method for NGC manufacture using a custom built laser-based microstereolithography (μSL) setup that incorporated a 405 nm laser source to produce 3D constructs with ~50 μm resolution from a photocurable poly(ethylene glycol) resin. These were evaluated by SEM, *in vitro* neuronal, Schwann and dorsal root ganglion culture and *in vivo* using a thy-1-YFP-H mouse common fibular nerve injury model. NGCs with dimensions of 1 mm internal diameter × 5 mm length with a wall thickness of 250 μm were fabricated and capable of supporting re-innervation across a 3 mm injury gap after 21 days, with results close to that of an autograft control. The study provides a technology platform for the rapid microfabrication of biocompatible materials, a novel method for *in vivo* evaluation, and a benchmark for future development in more advanced NGC designs, biodegradable and larger device sizes, and longer-term implantation studies.

© 2015 The Authors. Published by Elsevier Ltd. This is an open access article under the CC BY license (http://creativecommons.org/licenses/by/4.0/).

1. Introduction

Peripheral nerve injury is often a very serious, debilitating condition that affects 1 in 1000 patients [1—3]. In addition to the consequences of such injuries for the patient, it impacts considerably on health care expenditure, reduced employer output and loss of earnings. Due to the debilitating nature and prevalence of these types of injuries, there are a number of established techniques for the treatment of peripheral nerve repair. For small nerve injury gaps, the coaptation of the two severed nerve ends via direct suturing is common. For larger gaps this technique is frequently not possible or results in increased tension along the re-joined nerve, decreasing blood flow to the injury site, diminishing the regenerative capacity and overall surgical outcome [4]. In these cases autologous nerve grafts are the current gold standard [5], but are associated with a number of major disadvantages, including donor site morbidity and increased surgical complications.

An alternative approach to peripheral nerve repair of short injury gap is to utilise an implantable entubulation device known as a nerve guidance conduit (NGC). These devices are designed not only to act as a guide for the regenerating nerve end, but also to modulate the internal environment and to promote host regeneration [1,2,6]. A small range of commercially available devices exists, fabricated from FDA approved materials [1]. While these devices show similar efficacy to autograft surgery for short injury gap repair, their efficacy for gaps beyond ≈20 mm is limited [7]. This is believed to be due to their simple structural design, which for

* Corresponding author. Tel.: +44 (0)114 2225972.
** Corresponding author. Tel.: +44 (0)114 2717850.
*** Corresponding author. Tel.: +44 (0)114 2225513.
E-mail addresses: f.boissonade@sheffield.ac.uk (F.M. Boissonade), f.claeyssens@sheffield.ac.uk (F. Claeyssens), j.w.haycock@sheffield.ac.uk (J.W. Haycock).
[1] Authors contributed equally to this study.

commercial NGCs is a hollow tube, but also the bulk material properties. Synthetic NGC materials typically include polymers such as poly(lactic-co-glycolic acid) and their derivatives [8] and poly(caprolactone co-glycolic acid) [9]. The only naturally derived material used commercially to date is collagen [1], although spider silk is being investigated experimentally [10]), as are polymers produced by bacterial fermentation e.g. polyhydroxyalkoanates [11].

Commercial NGCs do not presently incorporate structures within the device lumen for potentially improving micro-structural guidance. This is partly due to the production techniques utilised and their need for scalability, which are typically of an extrusion or injection moulding approach. These have limitations in the ability to create feature sizes of micrometer dimensions for production of clinically relevant sized devices. This limits the ability to incorporate micrometer sized structural features in to the wall [12] or intra-lumenary space [13]. Intraluminal channel features and guidance scaffolds are being researched [2,14]. The incorporation of features experimentally by electrospinning or channel formation has been reported, with improved neuronal and Schwann cell organisation both in vitro [9,13,15,16] and in vivo [10,16–19]. Given these findings and the unique micro-structured organisation of peripheral nerve, a need exists for scalable fabrication techniques that extend beyond that of traditional extrusion processes for creating biocompatible nerve guides manufactured with micrometer resolution.

Microstereolithography (µSL) is an additive manufacturing technique offering the ability to produce devices with an intricate internal structure by solidifying a liquid photocurable resin via irradiation. If used in conjunction with a moveable stage, the technique provides an ability to control the region of irradiation and produce macroscopic scale objects. The technique is advantageous in the ability to create scaffolds and devices containing intricate microstructures using resin pre-polymers under CAD/CAM control. It is also amenable to scale-up for mass production upon optimisation of the processing conditions, with automated and simultaneous object production on the same setup. This technique is, however, currently limited to a small number of biocompatible materials, but is finding use in the moulding of biomaterials [20], and its ability to directly cure structures within a liquid pre-polymer greatly simplifies the fabrication technique.

The aim of this study was therefore to design a laser-based microstereolithography setup for the accurate fabrication of a basic-design experimental guidance conduit for peripheral nerve repair using a low molecular weight photocurable liquid pre-polymer based on poly(ethylene glycol) (PEG). Following fabrication, the dimensions of the NGC was assessed using scanning electron microscopy. The NGC materials were then tested in vitro using nerve cell cultures (neuronal cells, Schwann cells and dorsal root ganglion) and in vivo using a short gap repair model in thy-1-YFP-H mice (YFP+). The YFP+ transgenic mouse strain possesses a population of fluorescently labelled peripheral axons, which has enabled successful visualisation and quantification of axon regeneration across sites of nerve injury [21], but has not previously been used to assess NGCs. The present study is therefore the first to report on the manufacture of nerve guides out of a biocompatible material by 3D micro-structured printing, together with evaluation using in vitro and in vivo studies.

2. Materials and methods

2.1. Two dimensional material sample production using spin coating and UV irradiation

Two-dimensional samples were produced by first surface functionalising 13 mm glass coverslips with methacrylate groups by immersing samples for 30 min in a 3:1 sulphuric acid and hydrogen peroxide Piranha solution. Following this, the glass coverslips were washed in deionised water and dried before being immersed into a 10% (v/v) of methacryloxypropyltrimethoxysilane (MAPTMS) (Sigma–Aldrich, UK) in toluene for a minimum of 24 h. MAPTMS functionalised samples were washed in isopropanol (IPA) and dried immediately prior to mounting to the spin coating apparatus. Following this, a solution of photocurable poly(ethylene glycol) diacrylate (PEG-DA, 250 g/mol, Sigma Aldrich, UK), which is a viscous liquid at room temperature and in this context is the prepolymer, was prepared together with the addition of 2% (wt/wt) diphenyl-(2,4,6-trimethylbenzoyl)-phosphine oxide/2-hydroxy-2-methylpropio-phenone 50/50 (Sigma Aldrich, UK) photoinitiator, as described previously [22]. A small amount of solution was then added to a MAPTMS functionalised 13 mm glass coverslip using a glass pipette, the spin coater initiated and 3 s thereafter the sample was irradiated using an EXFO model S1000 100 W mercury arc lamp (Photonic Solutions Ltd, UK) ultraviolet light source for 30 s. Samples were subsequently washed three times and stored in fresh IPA until required for use. Immediately prior to use, the polymer-coated coverslips were removed from IPA and washed using sterilised PBS before transferring into a 12-well culture plate for in vitro cell culture.

2.2. In vitro cell culture of neuronal cells on 2D material surfaces

NG108-15 neuroblastoma × glioma rat/mouse hybrid neuronal cells (from Public Health England, Salisbury, U.K) were maintained in tissue culture polystyrene (TCP) treated T75 flasks using 10 mL Dulbecco's modified Eagles medium (DMEM, Biosera, UK) supplemented with 10% (v/v) foetal bovine serum (FBS), 0.25 µg/mL amphotericin, 2 mM L-glutamine, 100 units/mL penicillin and 100 µg/mL streptomycin. Cells were passaged after reaching a surface confluency of approximately 80% by mechanical removal from the culture surface. Cell number was determined by haemocytometer and a volume containing 1×10^5 cells was transferred into a fresh T75 flask along with 10 mL of culture medium. Neuronal cells were used experimentally within passages 15 to 25. In order to stimulate neurite extension, NG108-15 cells were cultured in DMEM supplemented with 0.25 µg/mL amphotericin, 2 mM L-glutamine, 100 units/mL penicillin and 100 µg/mL streptomycin (i.e. under serum-deprived conditions). For in vitro cell culture, seeding density was 25,000 cells per well (on 13 mm glass coverslips in a 24 well plate) for 12, 24 or 72 h in differentiation medium. Cells were cultured a humidified atmosphere incubator at 37°C (5% CO_2/ 95% air).

2.3. Three dimensional sample preparation using 405 nm microstereolithography

A 405 nm microstereolithography setup was used to fabricate three-dimensional structures, comprising of the following components: a Digital Micromirror Device (DMD) (Texas Instruments Incorporated, TX, USA), 100 mW 405 nm tunable laser source and associated proprietary software (Vortran Laser Technology Inc, Sacramento, CA, USA), motorised z-axis translation stage apparatus and attached metal stage (Thorlabs Ltd, Cambridgeshire, UK), controlled via proprietary software for the z-stage (APT Software, Thorlabs Ltd, Cambridgeshire, UK), as described previously [23]. The process and experimental setup is illustrated in Fig. 1. The DMD beam was expanded and the light pattern projected into the photocurable resin using an assembly of lenses and mirrors (Thorlabs Ltd, Cambridgeshire, UK). The lenses where aligned as such to produce a well-resolved image upon the fabrication stage. Bitmap images used for the fabrication process were created using commercially available software (e.g. Microsoft Paint). The size of the image displayed on the software was calibrated with the dimensions of the structure produced. This process involved producing an image of known pixel dimensions and measuring the resultant structure size.

In order to fabricate a structure, the liquid pre-polymer solution of PEG-DA (250 g/mol, Sigma Aldrich, UK) was prepared via the addition of diphenyl-(2,4,6-trimethylbenzoyl)-phosphine oxide/2-hydroxy-2-methylpropiophenone 50/50 (Sigma Aldrich, UK) photoinitiator at 2% (wt/wt) for the 405 nm laser and then vigorously shaken for 1 min before being thoroughly mixed for 15 min using an ultrasonic bath to ensure homogenous distribution of photoinitiator. The liquid pre-polymer PEG-DA solution was subsequently dispensed into a glass vial of a volume large enough to accommodate both the liquid and the stage upon which the construct was fabricated.

To produce a nerve guidance conduit from the PEG-DA prepolymer a cross section bitmap image of the fabricated structure was initially uploaded onto the DMD device using ALP-3 Basic version 1.0.03 (ViALUX, GmbH). To start the µSL experiment the laser shutter was opened and the z-axis translation stage set into operation. Once the stage descended to its intended depth a timed 3-s delay was introduced to allow the final section of pre-polymer to cure and laser shutter was closed. The main parameters influencing the structural quality of the NGC construct are the laser power and the z-translation speed. In general, the highest resolution structures were obtained with low input powers (1–5 mW) and low z-translation speeds (0.01–0.05 mm/s). After the µSL process was finished the metal stage was detached from the z-axis translation apparatus and immediately submerged into a large volume of denatured alcohol (90% ethanol/10% methanol). The structure was then removed from the metal stage using a scalpel. If fabricated structures were to be used for in vitro cell culture or for in vivo implantation, they were left for at least 72 h in ethanol to permit dissolution of the photoinitiator and to ensure that any unreacted pre-polymer had been completely removed from the surface of the sample prior to use.
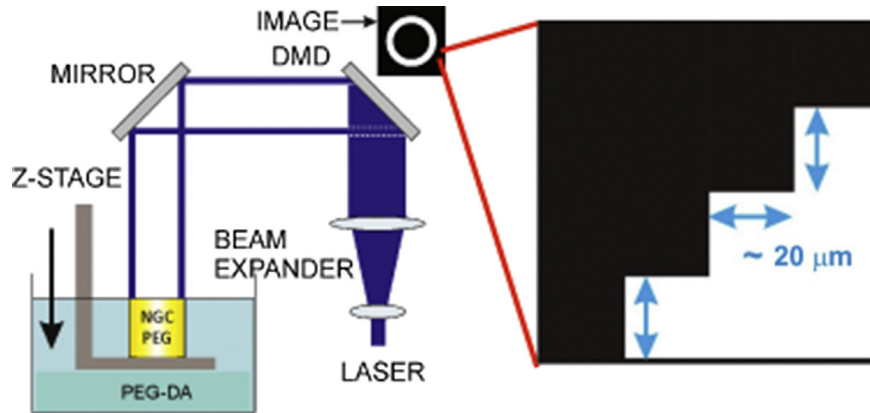
Fig. 1. Schematic diagram illustrating the microstereolithography approach used. A liquid pre-polymer PEG–DA solution plus photoinitiator were placed into a glass vial with an integrated a z-axis translation stage. To produce a nerve guidance conduit from the PEG–DA prepolymer a cross section bitmap image of the fabricated structure was uploaded onto the DMD device, the laser shutter opened and the z-axis translation stage set into operation. Once the stage descended to its intended depth a timed 3-s delay was introduced to allow the final section of pre-polymer to cure to PEG. Main parameters influencing the structural quality were laser power and z-translation speed. Highest resolution structures were obtained with low input powers (1—5 mW) and low z-translation speeds (0.01—0.05 mm/s). The surface topography of channels and tubes produced showed the presence of aligned grooves in the z-axis direction (showed in Fig. 3D), which arises via pixilation of the DMD device, which consists of 20 μm size mirrors on a 1:1 object-to-image size ratio.

2.4. Sample fabrication by microstereolithography

Two types of structures were fabricated: 1) channels for the culture of dorsal root ganglion explants for *in vitro* evaluation and 2) nerve guidance conduits for *in vivo* implantation and evaluation. Channels for the culture of dorsal root ganglion were produced (Fig. 3) using a 405 nm μSL setup from low molecular weight PEG-DA as described above. The design resulted in a 2 mm diameter half-circular trench within a 3.5 mm width, 2 mm height and 10 mm long rectangular block of PEG, with the bottom of the well having the same curvature of a 1 mm internal diameter tube. A number of different experimental designs were considered with varying dimensions of the nerve guidance conduit wall thickness, internal lumen diameter, overall length and outer wall diameter. This was primarily to permit selection of an optimum sized conduit for the *in vivo* nerve implant site. The internal diameter was selected to ensure a close fit to the entubulating nerve (the mouse common fibular nerve used in the *in vivo* injury model), while the wall thickness was optimised to be the minimum thickness to ensure good surgical handling. Smaller wall thicknesses rendered the NGC too fragile to handle, and the optimum size for implantation was deduced to be 1 mm in diameter, 250 μm in wall thickness and 5 mm in length for a 3 mm nerve injury gap (Fig. 3).

2.5. Mechanical testing of PEG nerve conduits

Conduits of 1 mm internal diameter, 250 μm wall thickness and 5 mm in length manufactured by microstereolithography above were mechanically tested by compression and analysed using a 450 N load cell in a Bose ElectroForce 3200 load frame system (Bose Ltd, Kent, UK). PEG conduits were placed vertically between two stainless steel compression plates (shown in Fig. 4a) and a compression rate of 0.1 mm/s was applied to the samples until failure occurred. Datasets of three independent nerve guide tests were collected, exported and analysed using Origin-Pro8 (OriginLab, Stoke Mandeville, Buckinghamshire, UK) with average Young's modulus, percentage compression to failure and maximum stress to failure calculated.

2.6. Dorsal root ganglion explant extraction and in vitro culture

Male Wistar rats were grown and sacrificed according to a schedule I procedure (cervical dislocation) in accordance to the Animals (Scientific Procedures) Act 1986. The animal was skinned and the complete spine was removed, cut longitudinally and with the aid of a dissection microscope the individual dorsal root ganglion (DRG) were extracted using fine tip forceps. The explants were then trimmed and placed onto the experimental culture substrate (NGC channel). The liquid surrounding the ganglion was removed using a 20 μL pipette, the lid fixed into place and placed into a tissue culture incubator at 37°C and 5% CO$_2$/95% air for 15 min. Subsequently, enough culture medium (comprised of DMEM supplemented with 10% (v/v) foetal bovine serum, 0.25 μg/mL amphotericin B, 2 mM glutamine, 100 units/mL penicillin and 100 μg/mL streptomycin) was carefully added to the well containing the NGC/DRG samples using a 1 mL pipette to cover the ganglion, taking care not to cause physical disturbance. Samples were cultured in a humidified incubator at 37°C (5% CO$_2$/95% air) for 14 days with a medium change every 72 h.

2.7. Immunolabelling of neuronal cells, Schwann cells and dorsal root ganglion

Cells were fixed by immersion in a solution of 3.7% (w/v) formalin (Sigma-—Aldrich Company Ltd, UK) in distilled water for 15 min and then washed by immersion in phosphate buffered saline **(PBS) three times.** Subsequently, cells were permeabilised by immersion in 0.1% (w/v) Triton X100 (Sigma—Aldrich Company Ltd, UK) in PBS and washed by immersion in PBS three times. **Samples were then blocked with 5 % (w/v) bovine serum** albumin (BSA) in PBS for 1 h at room temperature (RT). Subsequently, neuronal cells were immunolabelled with an anti-βIII tubulin primary mouse monoclonal antibody (Promega Corporation, Southampton, UK) at 1:500 in 1% (w/v) BSA in (PBS) for 1 h at RTP, followed by 3 × 15 min PBS washes. Samples were then immunolabelled with horse anti-mouse IgG secondary antibody conjugated to Texas Red (Vector Laboratories, Peterborough, UK) at 1:250 in 1% (w/v) BSA in PBS, followed by 3 × 15 min PBS washes. Schwann cells were immunolabelled with anti-S100β rabbit polyclonal IgG primary antibody (Dako UK Ltd, Cambridge, UK)) at 1:250 in 1% (w/v) for 1 h at RTP, followed by 3 × 15 min PBS washes. Samples were then incubated with a fluorescein conjugated goat anti-rabbit IgG secondary antibody (Vector Laboratories, Peterborough, UK) at 1:250 in 1% (w/v) BSA in PBS for 1 h, followed by 3 × 15 min PBS washes. The nuclei of all cells were labelled using 4′, 6-diamidino-2-phenylindole dihydrochloride (DAPI) at 300 nM for 1 h at RTP (Sigma—Aldrich Company Ltd, UK), followed by 3 × 15 min PBS washes.

2.8. Confocal and 2-photon microscopy of neuronal and Schwann cells

Images were acquired using a Zeiss LSM 510 META confocal microscope (Carl Zeiss Ltd, United Kingdom) with 543 nm and 488 nm excitation lasers. Additionally, a 2-photon mode-locked tuneable Ti-Sapphire laser was set at 750 nm emission (Chameleon Ultra III, Coherent Inc, Santa Clara, CA, USA) using Zeiss LSM Imager software. Three dimensional nerve channel structures containing DRGs cultured in standard 6-well plates were imaged in PBS *in situ* using a 10× magnification Zeiss W Plan Achromat water-dipping objective lens. For imaging Texas Red labelled samples incident and excitation wavelengths $\lambda_{ex} = 543$ nm/$\lambda_{em} = 576$ nm were used, and for imaging FITC-labelled samples incident and excitation wavelengths of $\lambda_{ex} = 488$ nm/$\lambda_{em} = 525$ nm were used. DAPI labelled nuclei were visualised using incident and excitation wavelength of $\lambda_{ex} = 750$ nm/$\lambda_{em} = 480$ nm. Images were captured as raw data files. Adobe Photoshop CS5.1 (Adobe Systems Incorporates, CA, USA), ImageJ (NIH, USA) or the ImageJ distribution Fiji (General Public Licence) post-processing software was used as detailed below (plugins used are indicated and cited).

2.9. MTT viability of neuronal cells

NG108-15 neuronal cell viability was measured using an MTT (3,4,5-dimethylthiazol-2,5-diphenyl tetrazolium bromide) assay. Cells were seeded on tissue culture plastic (TCP) and spin-coated PEG coverslips and in 12-well plates (1 mL, 1×10^4 cells/mL) for 24, 48 and 72 h. After each time point, culture medium was removed, cells were washed with PBS and 1 mL of MTT (0.5 mg/mL) solution was added. After 40 min the MTT solution was removed and 300 μL of acidified isopropanol (5 μL HCl in 5 mL isopropanol) was added. The formazan crystals resulting from MTT reduction were dissolved in ethanol and the solution mixed and transferred into 96-well plates. Absorbance was measured at 540 nm and referenced at 630 nm using a BIO-TEK ELx 800 microplate reader.

2.10. In vivo implantation of conduits in to a mouse common fibular nerve injury model

YFP+ mice were obtained from a Home Office approved UK supplier (JAX® Mice, Maine, USA via Charles River UK Limited, Margate, UK.) and bred for experimental

purposes. Experiments were carried out following UK Home Office project and personal licences, with local ethical approval, in accordance with the Animals (Scientific Procedures) Act 1986. Eighteen mice aged between 12 and 18 weeks old were used: 12 YFP+ and 6 C57B/6J (WT). WT mice were littermates of the YFP+ mice (as YFP+ mice are heterozygote for thy-1-YFP gene, so offspring without the gene revert to the wild type strain, C57B/6J). The experimental model involved unilateral repair of the common fibular nerve in YFP+ mice with either a polyethylene glycol conduit or a graft taken from a WT littermate. The PEG conduit repair group consisted of 6 YFP+ mice and the graft repair group − 6 YFP+ and 6 WT mice.

For conduit repair, YFP+ mice were placed under general anaesthesia (2−3% isoflurane; Abbot Laboratories, England) and the right common fibular nerve exposed and carefully freed from the surrounding tissue. The nerve endings were trimmed to create a gap of 3 mm between the proximal and distal ends and a PEG conduit positioned with approximately 0.25−0.5 mm of each nerve ending inside. Fibrin glue (equal quantities of fibrinogen, 10 mg/mL, and thrombin, 40 units/mL; Sigma−Aldrich, UK) was then applied to the site and allowed to set for 5 min in order to secure the nerve endings and conduit in position. Once the conduit was secured, muscle and skin were sutured and a single dose of analgesic administered (0.01 mL buprenorphine hydrochloride, 0.3 mg/mL; Vetergesic®, Alstoe Animal Health, UK) prior to the mouse being placed in an incubator to recover.

For graft repairs, a WT mouse was anaesthetised (Fluanisone, 0.8 mL/kg; Midazolam, 4 mg/kg; ip) and the right common fibular nerve exposed as in the conduit repairs. The nerve was then recovered with the surrounding muscle to prevent it from drying out and a YFP+ mouse was placed under general anaesthesia (2−3% Isoflurane; Abbot Laboratories, England) and the common fibular nerve exposed, freed from surrounding tissue and a silicone trough placed beneath to provide support for the nerve endings and graft during the repair. The nerve endings were trimmed to create a gap of 3 mm between the proximal and distal ends and a sufficient length of nerve was taken from the WT mouse, immediately trimmed to size and positioned in the silicone trough. The YFP+ nerve endings and WT donor nerve graft were then aligned and fibrin glue applied at each junction and allowed to set for 5 min before the silicone trough was carefully removed. In the YFP+ mouse muscle and skin were sutured and a single dose of analgesic administered (0.01 mL buprenorphine hydrochloride, 0.3 mg/mL; Vetergesic®, Alstoe Animal Health, UK) prior to the mouse being placed in an incubator to recover. The WT mouse was culled by cervical dislocation.

Following a recovery period of 3 weeks (21 days) mice were re-anaesthetized (Fluanisone, 0.8 mL/kg; midazolam, 4 mg/kg; ip) and the common fibular nerve/conduit site exposed and freed from surrounding tissue. The skin was sutured to a brass ring to form a pool, which was filled with 4% (w/v) paraformaldehyde for 30 min to fix the nerve *in situ*. Following fixation the nerve was excised and any superfluous tissue removed. In conduit repairs the conduit was carefully removed by cutting in half lengthways with microscissors, gently removing the nerve tissue and mounted on a microscope slide using Vectashield® and the mouse culled by cervical dislocation.

2.11. Image acquisition and processing

Images of nerves were acquired by fluorescence microscopy (Zeiss Axioplan2 Imaging microscope with QImaging QI Click camera) using Image Pro-Plus software. Images were acquired ($\lambda ex = 467–498$ nm/$\lambda em = 513–556$ nm) using a $10\times$ objective lens with 30×10 μm z-stack sections through the nerve. From this, composite images were constructed. To obtain images of the full length of the nerve, sections through the Z-axis were acquired from typically 8 to 10 adjoining microscope fields and composite images joined using Adobe Photoshop. The field of view number was sufficient to cover the length of the repair with a slight overlap. Minimal image processing with Adobe Photoshop was applied to the joined images used for analysis; this consisted of adjusting brightness/contrast and image exposure in order to improve axon clarity.

2.12. Image analysis

The interface between the proximal axon stump and the implant was determined by visual observation of the YFP fluorescent axons. A perpendicular line was drawn across the image at that point. Using this line at the repair start point as a reference, further lines were drawn at 0.5 mm intervals. One 0.5 mm upstream step was made and the remainder up to a 4.0 mm post-repair, which corresponded to the implant distal stump interface (chosen to ensure the full length of repair was covered). A 'sprouting index' was calculated for each interval by counting the number of axons at each interval and dividing by the number of axons at the 'pre-repair' proximal stump interval, corresponding to native nerve. This gave an indication of whether the number of axons at a specific point had increased or decreased and allowed direct comparison between repairs. Axons at the 4.0 mm interval were then traced back along their length to the graft start in order to calculate the number of unique axons successfully regenerating through the length of the graft. A total of 75% of the axons present at the 4.0 mm interval were traced and the trace finished either when the axons reached the repair start point or joined up with a branch point of a previously traced axon. In order to detect any differences in unique axon percentages throughout the entire length of the repairs, the number of unique axons at all other intervals was also calculated. Additional axons were traced at any

interval with fewer than 75% of axons traced. The shortest direct route between the repair start and the 1.5 mm interval was measured along with the length of the traced axons over the same distance. This was used to calculate the percentage increase in average axon length per repair across the most disrupted portion in a typical repair. A shorter average axon length indicates a reduction in disruption in the early stages of the repair.

2.13. Statistical analysis

Statistical comparisons between groups were made using GraphPad Prism (version 5.00 for Windows; GraphPad Software, San Diego, CA). For the sprouting index and axon tracing comparisons, a 2-way ANOVA with Bonferroni post-tests was performed and for axon disruption comparisons a 2-tailed Student's *t*-test was used. Differences were considered significant when $p < 0.05$.

3. Results

3.1. Biocompatibility and differentiation testing of photocured poly(ethylene glycol) using 2D neuronal cell culture

NG108-15 neuronal cells were cultured on spin-coated films of the photocured PEG, versus cells grown on tissue culture polystyrene (TCP) for comparison. Neuronal cells were grown for 2 days in serum-containing medium to permit adhesion and proliferation, followed by 1 day in serum-deprived deprived medium to encourage differentiation. Fig. 2A and B shows confocal micrographs of neuronal cells grown on flat TCP and spin-coated photocured PEG surfaces. Neuronal cell nuclei were directly labelled with 4′,6-diamidino-2-phenylindole (blue) and indirectly immunolabelled for the neuronal marker β-tubulin-III (red), which specifically identifies neurite formation. Qualitatively, no differences were observed between neuronal cells grown on TCP versus PEG at 24 or 48 h, but after 72 h less cells were observed. Measurement of
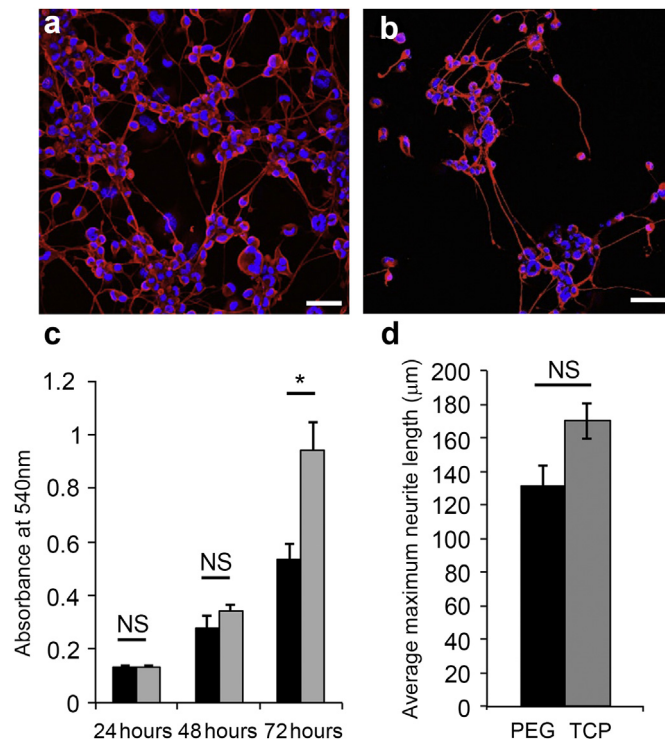
Fig. 2. Confocal micrograph images of NG108-15 neuronal cells grown on: (a) tissue culture polystyrene or (b) poly (ethylene glycol) for 72 h *in vitro* (bar = 100 μm). Nuclei were directly labelled with 4′,6-diamidino-2-phenylindole dihydrochloride (blue) and β-tubulin III immunolabelled (red) to reveal neuronal phenotype and neurite formation. (c) Metabolic viability assay (MTT) of NG108-15 cells grown on PEG compared to TCP after 24, 48 and 72 h of culture and (d) maximum neurite length of neuronal cells cultured on PEG versus TCP after 72 h.

cell viability was in broad agreement, with no significant difference in activity at 24 and 48 h, but a reduction on PEG compared to TCP at 72 h (Fig. 2C). Neuronal cell differentiation was also quantified, identified as maximum neurite length per neuronal cell, which revealed no significant difference between cells grown on PEG (mean ± SD = 131.2 ± 12.6 μm) versus TCP (mean ± SD = 170.2 ± 10.7 μm) at 72 h (Fig. 2D). Experiments were terminated at 3 days as neurite length is physically impaired at higher cell densities, preventing accurate interpretation.

3.2. Production of three-dimensional constructs by microstereolithography and mechanical testing

In order to permit evaluation of lithography structured devices prior to in vivo implantation, rat-derived dorsal root ganglion cultures were studied in vitro. To enable this, hemisphere 'trench' channel structures were produced (see Fig. 3C). The design comprised a 2 mm diameter half-circular channel within a 3.5 mm width, 2 mm height and 10 mm long rectangular block of PEG. The structure was devised so that the bottom of the well had the same curvature of a 1 mm internal diameter tube. This design also had

the advantage of being easily secured to the base of a standard 6-well culture plate, limiting its movement whilst in culture and permitted sample imaging using an upright fluorescent microscope without the need for preparative histology. The stereolithography process was optimised by comparing the reproducibility of micro-structures contained within the PEG cured objects (described below).

The same setup was used to build the nerve guidance conduits. Fig. 3A and B shows a poly(ethylene glycol) nerve guidance conduit fabricated using a 405 nm microstereolithography setup for implantation into a in vivo YFP fluorescent axon mouse peripheral common fibular nerve injury model. The resultant PEG was heavily cross-linked, with tubes undergoing no observable swelling upon immersion in water. The structures were 5 mm in length, outer diameter 1.5 mm and internal diameter 1 mm (hence a wall thickness of 250 μm). During the experimental optimisation, a protocol was devised to speed up production by arranging multiple images on the DMD. In this way five structures could be produce simultaneously. The time frame of the entire fabrication process took approximately 5 min including setting up the stage, structuring and polymerisation time and final washing, which equates to
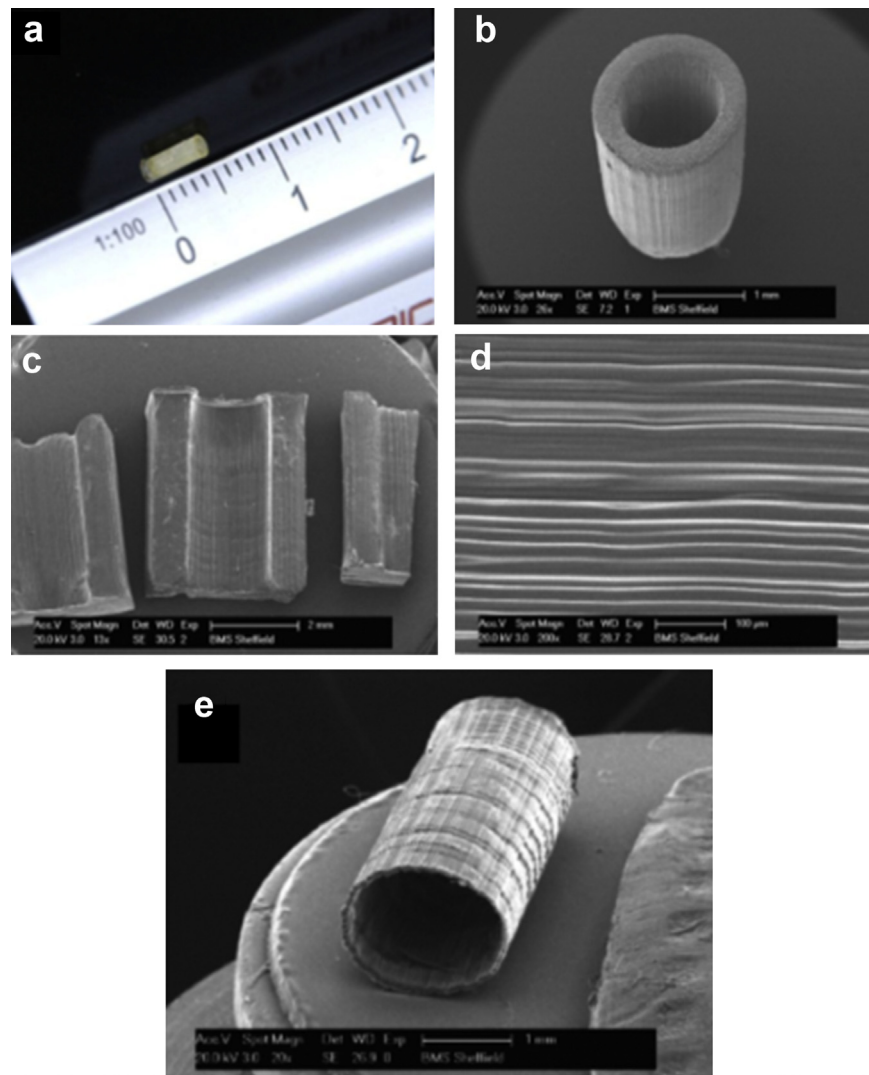
Fig. 3. (a) Optical and (b) scanning electron microscopy images of typical PEG nerve guidance conduits of 5 mm in length × 1.5 mm in diameter and a wall thickness of 250 μm (used in the in vivo analyses). (c) and (d) SEM images of a set of trenches 5 mm long, written with 5 mW laser power and a write speed of 0.01 mm/s, (c) at a magnification of 13× and (d) 200×. (e) An experimental PEG nerve guide made with a wall thickness of 50 μm to illustrate the resolution capability of microstereolithography.

a production rate of one structure per minute. This is of note and highlights a major advantage of projection microstereolithography as a production method, in that it is both a relatively rapid and up-scalable process upon construction and calibration of the equipment and processing conditions. Additionally, the dimensions of the conduits could be modified by adjusting the dimensions of the structure in cross section and images uploaded onto the DMD, without any additional changes to the setup.

Of interest, the surface microtopography of both the channels and the tubes showed the presence of aligned channel (or groove) features in the z-axis direction (Fig. 3D), which arose from the pixilation of the DMD device, which consists of 20 μm size mirrors on a 1:1 object-to-image size (illustrated in Fig. 1). This translated in to aligned printed microstructures of the same size as the individual mirrors. Thus, as the z-axis layers were written repeatedly, the result was a surface microstructure of parallel channels of the same magnitude. Reducing the object to image size reduced the pixilation effect and consequently the surface feature size observed, which in the illustrated structures were ≈20−25 μm in width, running along the long axis of the tube. When using optimal laser power and write speed conditions, the effect was found to be reproducible.

Mechanical testing of PEG nerve conduits is shown in Fig. 4, where conduits were placed vertically end-on and compressed at a rate of 0.1 mm/s (Fig. 4A). Conduits had an average Young's modulus of 470.0 ± 24.3 MPa, average percentage compression to failure of 4.5 ± 0.9% and an average maximum stress to failure of 11.46 ± 1.30 MPa. A typical profile of compression to failure is shown in Fig. 4B, illustrating the elastic region, yield and failure points. PEG conduits failed consistently by cracking. The data for each conduit (n = 3) and average values are shown in Fig. 4C.

3.3. In vitro cell culture − 3D dorsal root ganglion culture

The in vitro culture of DRG explants is a reported method for the assessment of peripheral nerve related devices, drugs and compounds. Our method utilised a 405 nm microstereolithography setup for the fabrication of specially designed in vitro culture channels, which allowed DRG bodies to be placed in the central channel. This experiment was designed to investigate the interaction of Schwann cells and neuronal cell neurites arising from the ganglion cell body with the photocured PEG used for the device. If the photoinitiator used for fabrication, the PEG-DA itself or any remaining unreacted pre-polymer produced a localised toxic environment this would result in very limited cellular adhesion or migration from the DRG body.

Fig. 5A shows a 2-photon composite z-projection image of a rat-derived spinal DRG cultured on a 405 nm fabricated PEG channel for 14 days. S100β labelling of Schwann cells was identified in green and β-tubulin-III labelling of neurites in red. Nuclei were labelled using 4′,6-diamidino-2-phenylindole. It was observed that the DRG body attached to the PEG channel culture surface, indicating adherence to the culture surface. Positive labelling of Schwann cells identified a maximum migration distance of 9.5 mm either side of the cell body after 14 days (Fig. 5B, tiled images, not to linear scale). It was also observed that many Schwann cells and neurites had migrated distally from the DRG body and had adhered to the sides of the PEG channel. A smaller DRG body extension was observed growing outwards with a cone shape along the base of the channel. These extensions were also identified arising from the larger DRG body, interacting with the material surface in the 3D rendered images (Fig. 5B). The directed migration of these features was

Tube number	Youngs modulus (MPa)	% Compression to failure	Maximum stress to failure (MPa)
1	497.1	5.3	12.65
2	462.9	4.8	10.08
3	450.1	3.5	11.65
Mean	470.0	4.5	11.46
Standard deviation	24.3	0.9	1.30
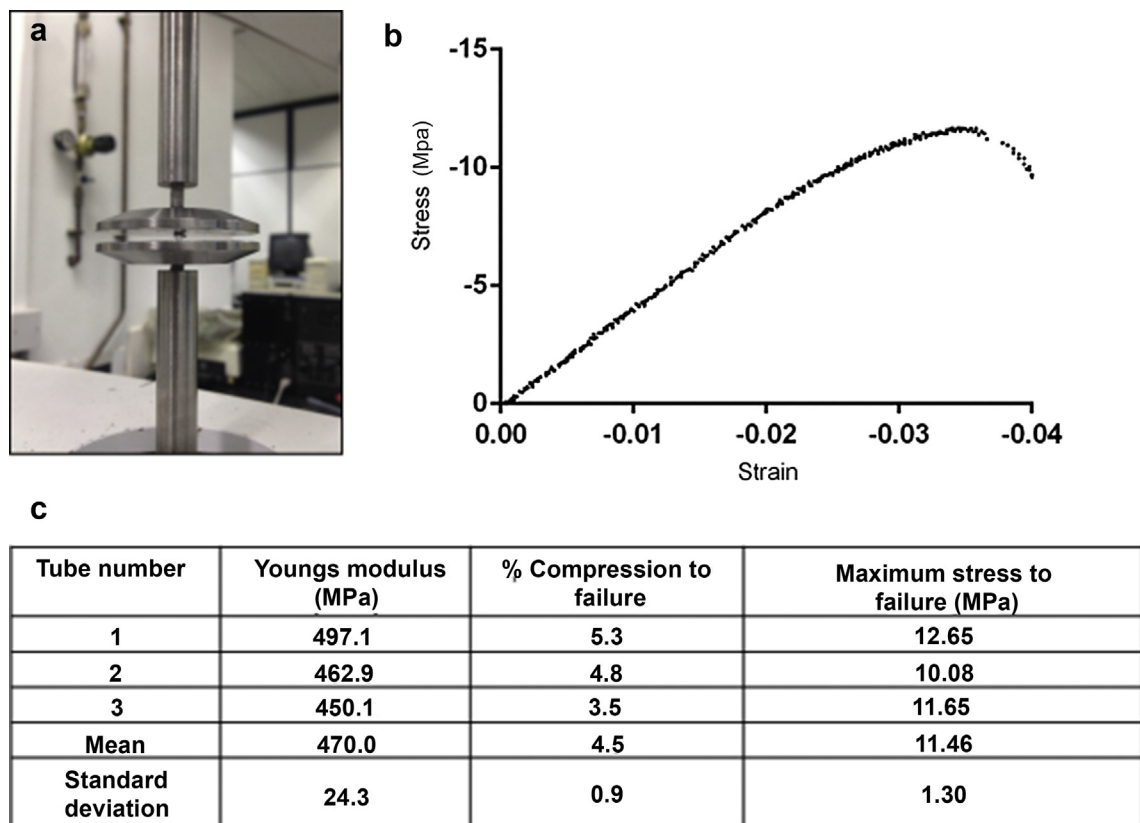
Fig. 4. (a) Mechanical compression testing was undertaken by placing conduits vertically end-on using a 450 N load cell in a Bose ElectroForce 3200 and a compression rate of 0.1 mm/s applied. (b) A typical stress (MPa) strain curve illustrating the elastic region, plastic region, yield point and fracture point. (c) Data for each conduit (n = 3) and the average values of Young's modulus, percentage compression to failure and maximum stress to failure (MPa) are shown.
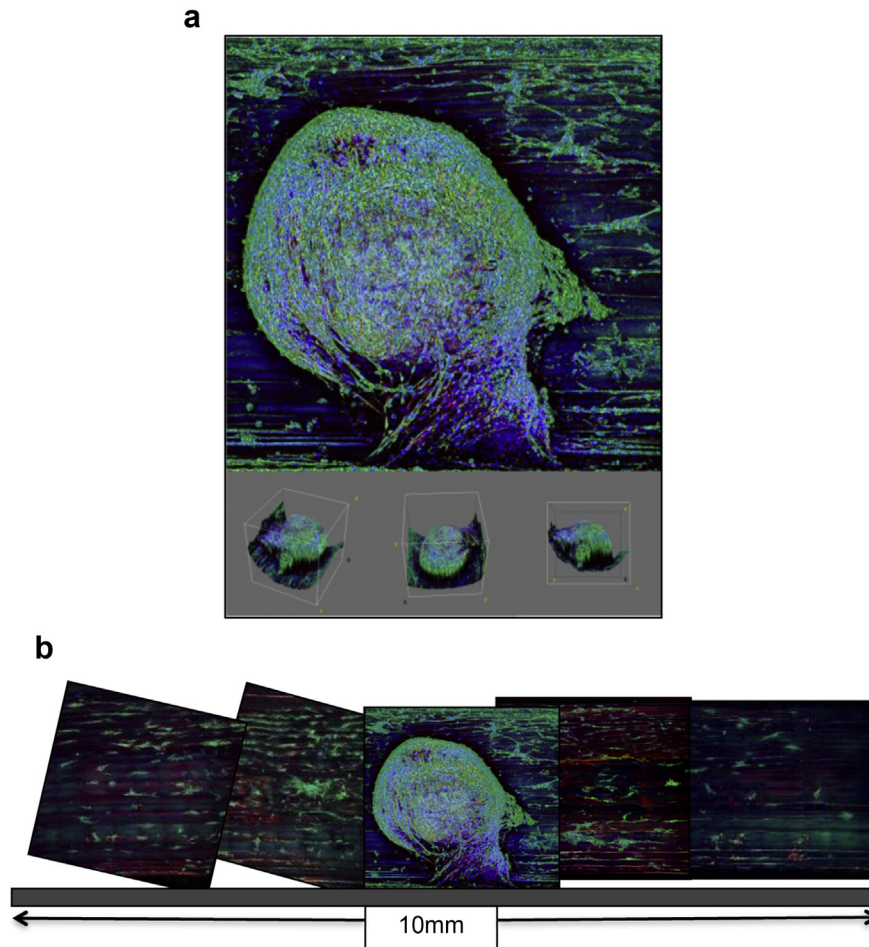
Fig. 5. (a) 2-photon microscopy z-projection of a rat dorsal root ganglion explant cultured *in vitro* for 14 days on a PEG channel fabricated by microstereolithography (illustrated in Fig. 3c) showing ganglion body adhesion, and lateral neurite and Schwann cell migration. Nuclei were directly labelled with 4′,6-diamidino-2-phenylindole dihydrochloride (blue), β-tubulin III immunolabelled to reveal neurite formation (red) and S100β immunolabelled to reveal Schwann cells (green). (b) A tiled image showing the relative position of the ganglion along the 10 mm length of the channel (not to linear scale).

presumed to arise due to the presence of the ≈20−25 μm parallel channels identified in the lumen wall (Fig. 3D).

3.4. YFP+ mouse common fibular short gap injury model

Implantation of a PEG guidance conduit in to a 3 mm mouse common fibular injury site is illustrated in Fig. 6A. All animals recovered well from the initial surgery with no signs of autotomy or infection. In graft-based control repair, disorganised axons were frequently observed at the interface between the proximal nerve ending and the graft, and this was observed in all graft repairs in the present study (Fig. 6B, Fig. 7 and Fig. 8). Once axons entered the graft they appeared to return to a similar level of organisation as observed at the proximal injury site. A small amount of disruption was observed at the join between graft and distal nerve ending, compared to the join at the proximal nerve ending, with axons returning to a more organised level once inside the distal nerve ending (Fig. 6B and Fig. 8A). In PEG conduit repairs, a similar level of disruption to that of the graft repair was observed at the interface between proximal nerve ending and the start of the conduit (Fig. 8A and B). It was observed that axons were generally less organised, compared to axons within grafts, as they progressed towards the distal nerve ending. Upon entering the distal stump, axons returned to a more organised state, similar to that observed in the graft (Fig. 8B).

Sprouting index analysis indicated no significant difference in terms of axon number between the PEG conduit or graft-based repairs at any single interval from the repair start to the distal nerve end (Fig. 9). Sprouting index values for PEG conduit repairs were slightly lower consistently than graft repairs at each measured interval between 0.5 mm and the distal nerve end, resulting in a significantly lower ($p = 0.047$) overall sprouting index profile for conduit repairs (Fig. 9). Sprouting index values were maximal in both repair types at the 0.5 mm interval ($145.4 \pm 8.6\%$; mean $\pm$ SEM) for conduit repairs and $170.4 \pm 15.3\%$ for graft repairs, before falling to their lowest values at the final (4.0 mm) interval ($48.6 \pm 11.1\%$) for conduit repairs and $65.3 \pm 8.9\%$ for graft repairs (Fig. 9).

When comparing the proportion of axons at the repair start (0.0 mm interval), represented at subsequent intervals, there was no significant difference between the PEG conduit and graft repair at any interval (Fig. 10). Almost 50% of axons from the 0.0 mm interval were lost by the 1.5 mm interval ($49.9 \pm 4.0\%$) in conduit repairs and $49.2 \pm 7.4\%$ in graft repairs and at the distal nerve ending interval (4.0 mm) only $16.5 \pm 3.9\%$ versus $20.5 \pm 3.8\%$ of axons from the 0.0 mm interval were represented in conduit and graft repairs, respectively (Fig. 11). The level of axon disruption across the initial portion of the repair was significantly lower ($p = 0.035$) in conduit repairs than in graft repairs, with an average increase in axon length of $11.4 \pm 1.8\%$ in PEG conduit repairs compared with $21.5 \pm 3.7\%$ in graft repairs (Fig. 12).
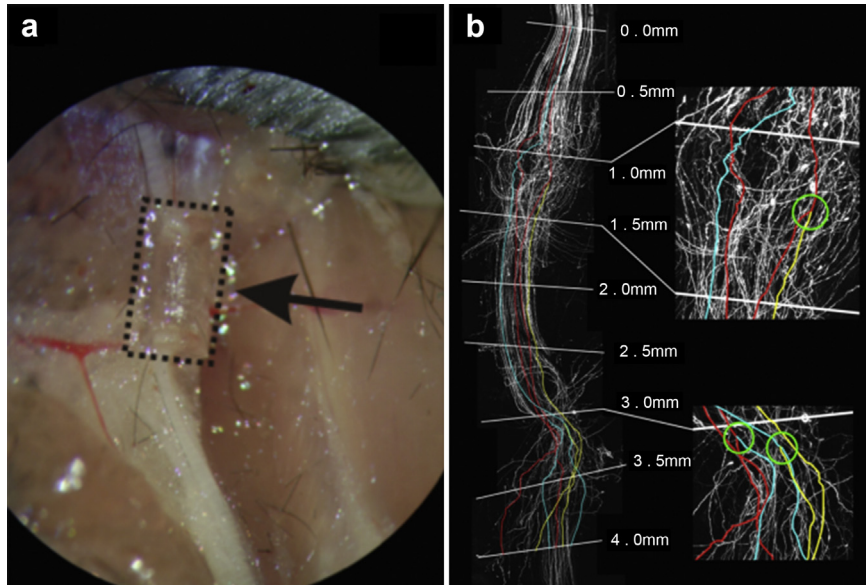
Fig. 6. (a) Implantation of a 5 mm × 1.5 mm × 250 μm PEG guide in to a THY-1-YFP-H common fibular mouse small gap 3 mm injury model. (b) Thy-1-YFP-H nerve graft repair image. Analysis method illustrating intervals marked with sample axon tracing from 4.0 mm interval position back to 0.0 mm (start) interval. The number of axons at each interval were counted and compared with a −0.5 mm interval (not shown) to obtain a sprouting index value; axons were traced from distal intervals back to 0.0 mm or a branch point with a previously traced axon (as highlighted in expanded sections with green circles) to calculate percentage of unique start axons represented at each interval.

4. Discussion

The major aim of this study was to develop a method of fabricating nerve guide devices by a rapid production approach, with an ability to obtain feature size and structural resolution that improves significantly on the more standard methods of microinjection or microextrusion moulding. We report on the production of nerve conduits by projection micro-stereolithography of a photocurable liquid resin in the form of a PEG-diacrylate prepolymer. This work builds on our previous work on the synthesis and use of photocurable materials for micro-stereolithography, including 2-photon polymerisation, for neural tissue engineering applications [24,25].

A small number of previous studies have reported on the use of PEG as a nerve guide. For example, Arcaute at al. highlight the processing of photocurable PEG hydrogel formulations (containing 20% water) into single and multilumen nerve guidance conduits with a very similar micro-SL setup as used in this study [26]. They report on the structural and mechanical properties of NGCs and also discuss the processing of PEG with embedded cells [27]. Very recently, Beke et al. reported the production of 3D scaffolds of a polypropylene fumarate:diethyl fumarate blend with a pulsed excimer laser for the production of nerve guidance conduits [28].
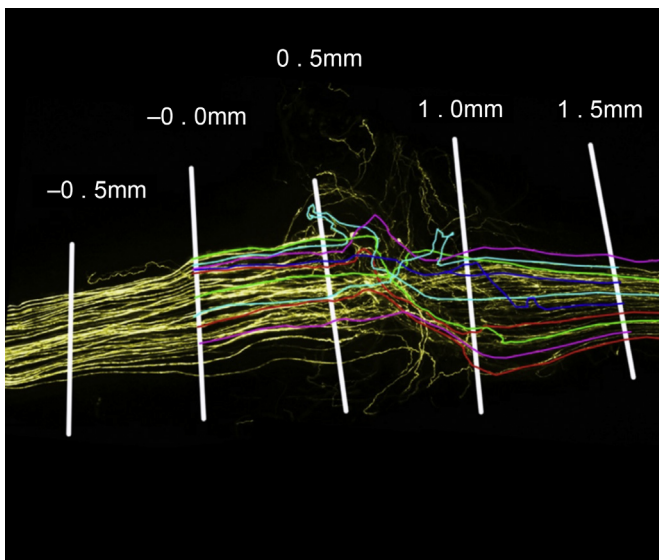
Fig. 7. Enlarged view at the interface between the proximal nerve ending and graft. Traced axons were measured and lengths compared with a direct route from 0.0 mm to 1.5 mm to determine an average increase in length.
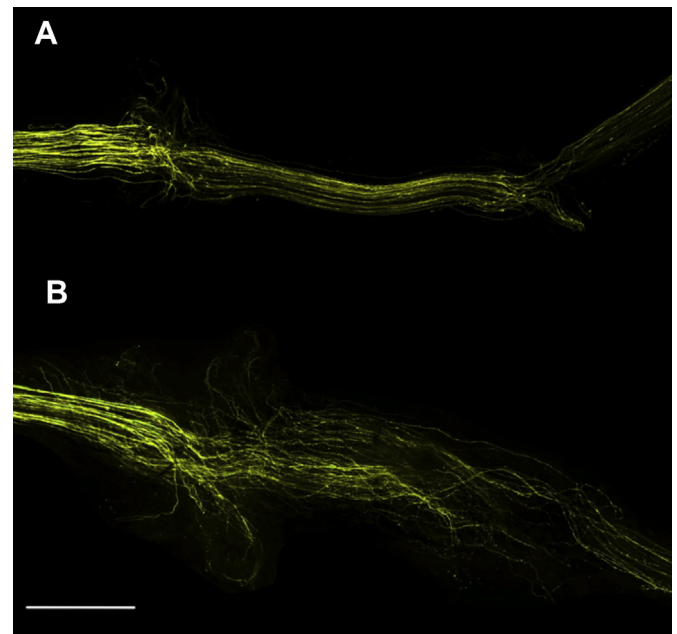
Fig. 8. (A) Typical graft repair and (B) implanted PEG nerve guide showing the respective organisation of regenerated axon paths (scale bar = 1.0 mm).
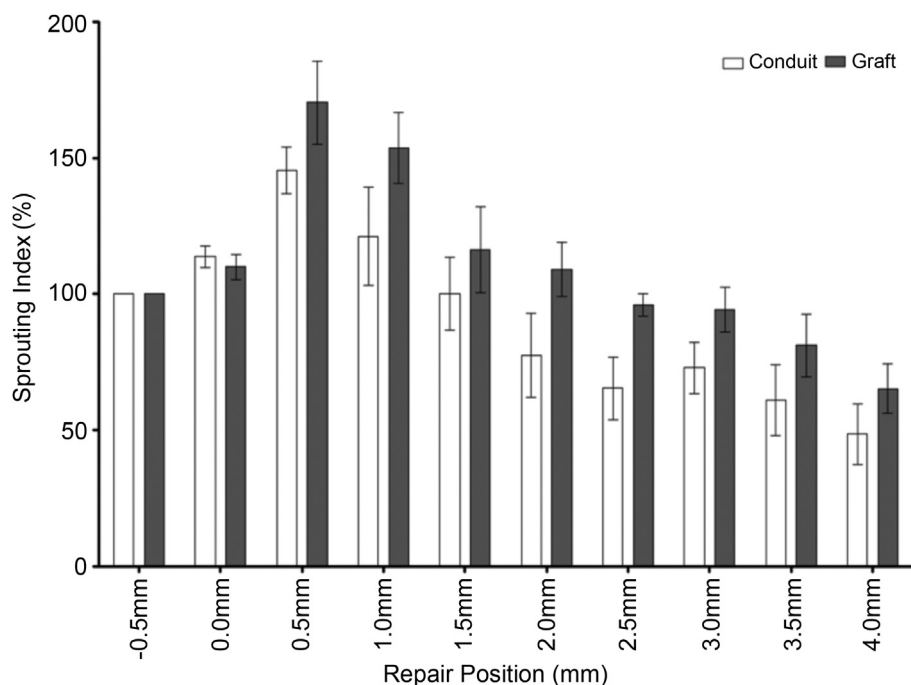
Fig. 9. Sprouting index values for each 0.5 mm interval. Overall profile of sprouting index values was significantly different $-p = 0.047$ (2-way ANOVA with Bonferroni post-tests).

However, these studies only report scaffold fabrication and to our knowledge stereolithographically produced scaffolds have never been implanted in an animal nerve injury model previously.

The peripheral nervous system has a phenotypic ability to repair if injured, in contrast with that of the central nervous system. Surgical intervention is required and approaches include autografts, allografts and nerve guidance conduits. Nerve guides have been a well-researched area in the last three decades, but despite this there are currently few products on the market, with a relatively modest ability to support neural regeneration [1]. Nerve guides are a promising alternative to autografts, but regeneration of the proximal axons is limited typically to gap injuries of less than 20 mm (reviewed in Refs. [1,2]). Researchers have focused on a wide range of approaches for increasing regeneration distance, with strategies aimed at improving the conduit, e.g. fabrication of devices made from materials more suitable for regeneration (e.g. poly(3-hydroxybutyrate) [29]), or containing coatings (e.g. ECM [30] or plasma polymers [31,32]). More advanced therapies are also well documented where the conduit is used to deliver growth factors (e.g. neurotrophin-3/neurotrophin-4 [33]), cytoprotective agents [34], the inclusion of internal guidance structures (as channels [19,35] or fibres [31,36—38]) and where the conduit is used in combination with a cell therapy, including the local delivery of support cells for stimulating proximal axon regeneration (e.g. Schwann cells [39,40]) or adult-derived stem cells, both as bone marrow-derived mesenchymal [41] or adipose-derived cells [42—45]).

We demonstrate herein the construction of a laser sourced microstereolithography setup with the capacity for producing devices intended for peripheral nerve repair. The system currently has an ability to produce written feature sizes as small as 50 μm while producing macro-scale structures as large as 15 mm. PEG when spun cast in the photocurable form supported the growth and experimental differentiation of neuronal cells. This was extended in to making semi-circular channels, which were able to support the growth and differentiation of dorsal root ganglion and the simultaneous adhesion and lateral migration of Schwann cells associated

with the explant, along pixelated microchannels of 20—25 μm width in the internal conduit wall. Thereafter, nerve guide conduits were constructed as 5 mm (L) × 1.5 mm (W) × 250 μm (wall thickness) devices. These had acceptable handling properties during implantation in to a mouse thy-1-YFP common fibular nerve short 3 mm gap injury model, and regeneration was almost comparable with an autograft control after 21 days implantation.

We found no significant difference in sprouting index values between conduit and graft repairs at any individual intervals, although levels were lower at the distal end in the conduits. This was related to a lower initial sprouting percentage, indicative of reduced disruption faced by the regenerating axons. The proportion of unique axons at the distal end in each repair group was also similar (not significant), indicating that functional recovery may be similar in both repair types. Axon-sprouting index profile in conduit repairs was significantly lower to that of nerve grafts, indicating that regeneration into the conduits was less disrupting for the axons. Previous studies have shown increased axon sprouting to be associated with increases in disruptive nerve damage [46]. The potential for lower disruption in conduit repairs was also indicated by the significantly lower increase in axon length across the initial portion of the repair compared to that of graft repairs. We did note increased variation between conduit repairs compared to graft repairs, indicating that regeneration through conduits was less predictable than in grafts. Additionally, axons in the conduit repairs appeared to lack organisational support in the gap between proximal and distal nerve endings, supporting the potential need for inclusion of intraluminal structures within a device.

The fabrication of structures down to 50 μm was demonstrated by a thin walled experimental PEG conduit shown in Fig. 3E. This device was not suitable for implantation due to its delicate nature, but it highlights the potential of the technique for producing macro-scale devices with a micro-scale structure. In comparison with other previously published stereolithography systems this is approximately ten times smaller in scale [47]. The ability to produce conduits with 50 μm wall thicknesses is of particular interest
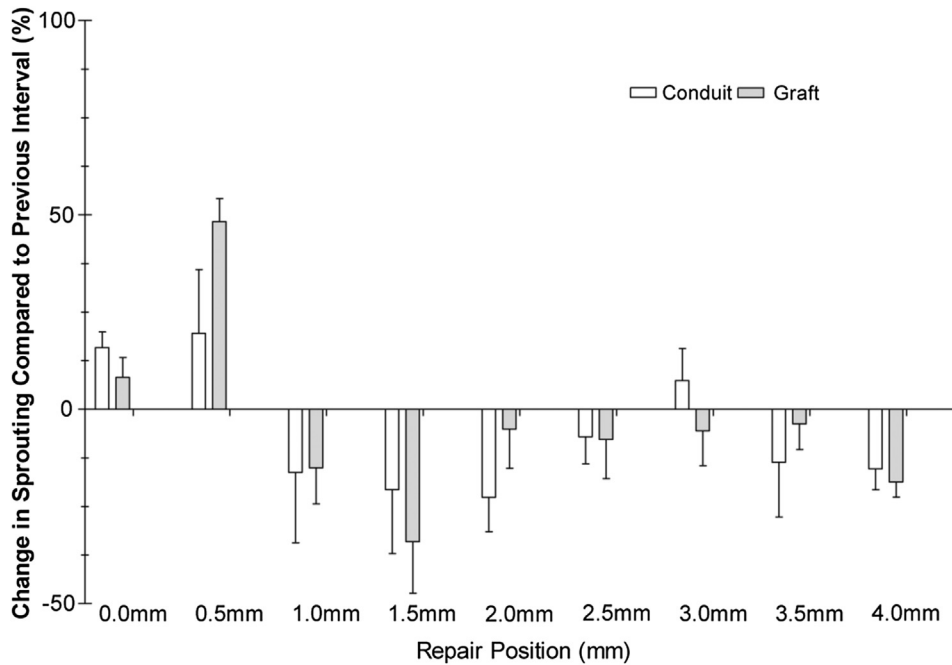
Fig. 10. Change in sprouting index values compared to previous 0.5 mm interval. No significant differences between conduit and graft repairs were found − $p > 0.05$ (2-way ANOVA with Bonferroni post-tests).

for nerve guidance conduits mainly because the strength of the conduit can be tailored accurately with small changes to the wall thickness by simple alteration to the CAD design. If the overall diameter of the nerve guidance conduit is close to that of the original nerve, the impact the extra volume created by implantation of the device will minimise injury at the host site. This is especially important for peripheral nerve injury sites, where patient limb movement has the potential cause further damage.

The commercial availability of PEG and ease of processing in a photocurable form makes it a biomaterial of choice for photolithography. PEG is typically an anti-fouling hydrophilic material (e.g. Ref. [48]), and ethylene oxide (or glycol) oligomers bound onto
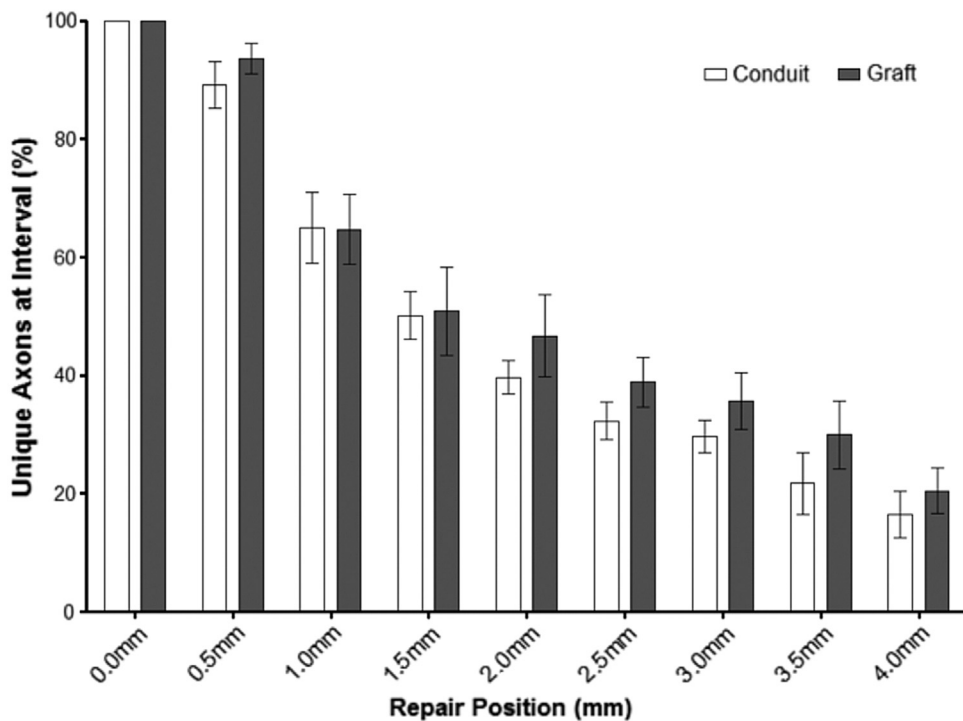
Fig. 11. Unique axons from the repair start (0.0 mm interval) represented at each distal interval. No significant differences were detected between conduit and graft repairs overall or at any individual intervals − $p > 0.05$ (2-way ANOVA with Bonferroni post-tests).
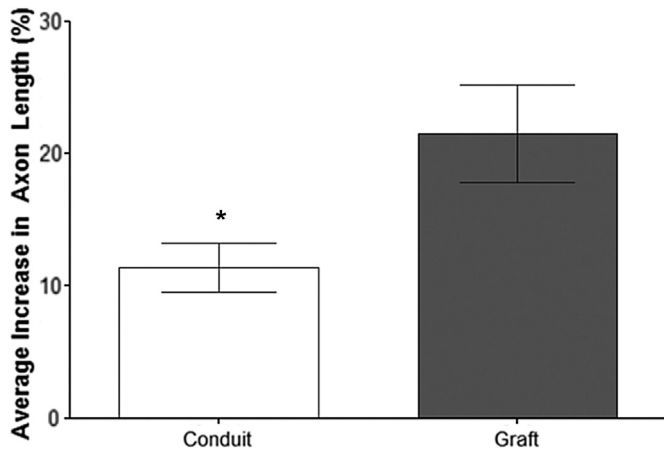
Fig. 12. Axon disruption across the initial 1.5 mm of repairs. Average increase in axon length in conduit repairs (11.4 ± 1.8%) was significantly lower than in graft repairs (21.5 ± 3.7%; p = 0.035; 2-tailed t-test).

surfaces as poly(ethylene oxide) or PEG brushes are known to act as extremely low-fouling surfaces [49]. However, these anti-fouling properties do not completely transfer to bulk objects produced from PEG-diacrylate. The surface of objects made from low molecular weight (Mw: 250 g/mol) PEG-diacrylate as conducted herein can be rendered protein and cell adherent after prolonged washing, and we have previously shown photocured PEG supports neuronal cell growth [50] [22], where the extent of adhesion is dependent on the PEG formulation, in particular the PEG-prepolymer chain length.

The rationale that nerve guides should degrade after implantation is supported by data showing that a breakdown rate of 18–24 months matches the rate of tissue regeneration [29]. While it is not generally accepted to use non-degradable nerve guide materials, the use of PEG as a non-degradable material may have clinical applicability for certain specialist repairs (e.g. lingual nerve reconstruction). In the present study it was used predominantly as an experimental material for developing micro-sterolithography, and as a basis for manufacturing nerve guides out of more clinically relevant and also degradable materials in the future. Notwithstanding, a number of approaches to render PEG biodegradable have been reported in the literature, most commonly by incorporating degradable cross-linkers or protein fragments [51–53]. Fragments typically under Mw 20,000 g/mol are eliminated from the body readily, compared to higher molecular weights > 40,000 g/mol [54].

The use of a digital micro-mirror for microstereolithography, which introduces pixilation, resulted in parallel microgrooves of ≈20–25 μm width that ran the length of the PEG conduit. We found it was possible to exploit this, where neurite guidance and Schwann cell migration arose in a longitudinal direction via contact guidance. Features have previously been designed in to implants, e.g. in the case of neuronal outgrowth experimental studies (e.g. Ref. [55]), where data supports the premise that microgrooved surfaces with feature sizes under 50 μm guide Schwann cell and neuronal outgrowth most effectively. We have previously established, amongst others, that neuronal and Schwann cells can be guided along aligned parallel electrospun fibres of 1–8 μm fibre diameters, where larger fibre diameters were more supportive [38]. Additionally, we have shown that neuronal cells extend along ≈10 μm lines built by 2-photon polymerisation [25]. The current study provides more evidence in support of this, and that adherence and outgrowth of DRG neurites and Schwann cells was observed, indicates that the bulk PEG material and internal wall

topography supported lateral growth and migration along the grooved surface.

The present study is also the first to use a YFP+ mouse strain to assess regeneration in nerve guide conduits, and the peripheral nerve injury model was found to have a particular advantage for the study of nerve conduits. By using YFP+ mice it was possible to directly visualise and quantify regeneration of individual axons across the repair site, without histological post-processing of samples. This ability to view the path taken by individual axons through the injury site allowed differences between conduit and graft repairs to be observed and quantified, including axonal organisation, which would not be possible using other nerve injury models. We decided to use a graft repair as a control to compare the performance of the nerve guide conduit, as the graft acts as a biological scaffold to guide the regenerating axons. Any portions of axons within the graft also degenerate and therefore do not contribute to the regeneration process. An alternative approach of a gap control was not considered an option, as this would not be chosen clinically. Fibrin glue was used for both graft and conduit repairs and is an established method for repairing peripheral nerves, and has no more detrimental effect on regeneration than the alternative of suture repair [56]. In this particular injury model the relatively small size of the peripheral nerve being repaired necessitated the use of fibrin glue over suture repair.

We have previously used functional measures such as electrophysiology and gait analysis to assess nerve regeneration in previous studies (e.g. Ref. [57]). Although electrophysiological testing would give indications of the number and size/maturity of axons crossing the repair site in the present study, it would be unlikely to reveal details such as axon disruption or disorganization. In particular, the results indicated that no differences would have been revealed in this study between nerve conduit and graft repairs using electrophysiology, as axon numbers reaching the distal nerve ending were similar in both repair types. In addition, the size and location of the common fibular nerve would make electrophysiological testing almost impossible, as the position of the stimulating electrodes would be impeded proximally by the branching of the sciatic nerve and distally by the nerve passing around the knee joint.

A major challenge in medical device design and regenerative medicine scaffolds is the desire to include structures at micrometer length scales in a bespoke, reproducible and controllable manner. This is currently a limitation of existing production technologies (e.g. injection moulding and extrusion) that fabrication techniques such as microstereolithography enables. The ability to 3D print biocompatible materials is very much in its infancy, and before we see a future where one can routinely print such biocompatible devices, it is necessary to develop biocompatible materials that are photocurable. However, such materials are currently limited to PEG, PLA and PCL. The future direction of this work is to use direct write techniques with more clinically relevant and/or biodegradable materials. This is in conjunction with precise control over the physical dimensions of the NGC bulk material, the incorporation of intraluminal structures and the ability to use materials where control over the Young's modulus is possible. In the current study an average Young's modulus of 470 MPa was measured by compression testing to destruction. Given that the Young's modulus of native sciatic nerve is approximately 0.5 MPa [58], we suggest that future materials with a modulus approaching nerve, but importantly able to physically support a regenerating wound, while enabling flexibility and surgical handling, are important future goals. Therefore a requirement to synthesise a wider range of low molecular weight photocurable pre-polymers which remain in the liquid phase at room temperature exists, and which can be cured by a UV/violet laser. In addition, extension of the current

work to the use of a larger *in vivo* gap injury model, together with longer implantation times will be necessary. Such work is currently in progress and will be published in due course.

5. Conclusions

In summary, we report on the construction of a laser sourced microstereolithography setup with the capacity for producing devices intended for peripheral nerve repair. The system can achieve a lower size resolution of 50 μm and in the current study produced devices 5 mm in length. While PEG is not typically conducive for cellular attachment, we observed that the photocurable form of PEG used herein was permissive for neuronal growth and experimental differentiation *in vitro*. Devices constructed from the bulk material had acceptable handling properties and performed comparatively with an autograft control in a thy-1-YFP-H mouse 3 mm gap injury model after 21 days, with the number of unique axons at the distal end in each repair group being similar. Variation between the conduit repairs was greater than in the graft repairs, highlighting a less predictable regeneration process and supporting the basis for intraluminal structures. Overall, the study highlights the potential of stereolithography for the rapid production of precise and intricate nerve guide structures, which permits individual customisation. This study also demonstrates the first use of the thy-1-YFP-H mouse to assess regeneration through nerve guide conduits. Future development of this technology is now underway using biodegradable materials, the incorporation of intraluminal structures, fabricating larger devices and the study of larger injury gap models using longer implantation times. In the future, this approach will have distinct advantages for the production of clinically relevant devices.

Acknowledgements

References

[1] Bell JH, Haycock JW. Next generation nerve guides: materials, fabrication, growth factors and cell delivery. Tissue Eng Part B Rev 2011;18(2):116−28.
[2] Daly W, Yao L, Zeugolis D, Windebank A, Pandit A. A biomaterials approach to peripheral nerve regeneration: bridging the peripheral nerve gap and enhancing functional recovery. J R Soc Interface 2012;9:202−21.
[3] Taylor CA, Braza D, Rice JB, Dillingham T. The incidence of peripheral nerve injury in extremity trauma. Am J Phys Med Rehabil 2008;87:381−5.
[4] Clark WL, Trumble TE, Swiontkowski MF, Tencer AF. Nerve tension and blood flow in a rat model of immediate and delayed repairs. J Hand Surg Am 1992;17:677−87.
[5] Haftek J. Autogenous cable nerve grafting instead of end to end anastomosis in secondary nerve suture. Acta Neurochir 1976;34:217−21.
[6] Jiang X, Lim SH, Mao H-Q, Chew SY. Current applications and future perspectives of artificial nerve conduits. Exp Neurol 2010;223:86−101.
[7] Kehoe S, Zhang XF, Boyd D. FDA approved guidance conduits and wraps for peripheral nerve injury: a review of materials and efficacy. Injury 2012;43: 553−72.
[8] Sundback CA, Shyu JY, Wang Y, Faquin WC, Langer RS, Vacanti JP, et al. Biocompatibility analysis of poly(glycerol sebacate) as a nerve guide material. Biomaterials 2005;26:5454−64.
[9] Bockelmann J, Klinkhammer K, von Holst A, Seiler N, Faissner A, Brook GA, et al. Functionalization of electrospun poly(epsilon-caprolactone) fibers with the extracellular matrix-derived peptide GRGDS improves guidance of Schwann cell migration and axonal growth. Tissue Eng Part A 2011;17: 475−86.
[10] Radtke C, Allmeling C, Waldmann KH, Reimers K, Thies K, Schenk HC, et al. Spider silk constructs enhance axonal regeneration and remyelination in long nerve defects in sheep. Plos One 2011;6(2):e16990.
[11] Bian YZ, Wang Y, Aibaidoula G, Chen GQ, Wu Q. Evaluation of poly(3-hydroxybutyrate-co-3-hydroxyhexanoate) conduits for peripheral nerve regeneration. Biomaterials 2009;30:217−25.
[12] Aebischer P, Guénard V, Valentini RF. The morphology of regenerating peripheral nerves is modulated by the surface microgeometry of polymeric guidance channels. Brain Res 1990;531:211−8.
[13] Dubey N, Letourneau PC, Tranquillo RT. Guided neurite elongation and Schwann cell invasion into magnetically aligned collagen in simulated peripheral nerve regeneration. Exp Neurol 1999;158:338−50.
[14] Bellamkonda RV. Peripheral nerve regeneration: an opinion on channels, scaffolds and anisotropy. Biomaterials 2006;27:3515−8.
[15] Wang HB, Mullins ME, Cregg JM, McCarthy CW, Gilbert RJ. Varying the diameter of aligned electrospun fibers alters neurite outgrowth and Schwann cell migration. Acta Biomater 2010;6:2970−8.
[16] Chew SY, Mi R, Hoke A, Leong KW. The effect of the alignment of electrospun fibrous scaffolds on Schwann cell maturation. Biomaterials 2008;29:653−61.
[17] Chew SY, Mi R, Hoke A, Leong KW. Aligned protein-polymer composite fibers enhance nerve regeneration: a potential tissue-engineering platform. Adv Funct Mater 2007;17:1288−96.
[18] Schnell E, Klinkhammer K, Balzer S, Brook G, Klee D, Dalton P, et al. Guidance of glial cell migration and axonal growth on electrospun nanofibers of poly-epsilon-caprolactone and a collagen/poly-epsilon-caprolactone blend. Biomaterials 2007;28:3012−25.
[19] Daly WT, Yao L, Abu-rub MT, O'Connell C, Zeugolis DI, Windebank AJ, et al. The effect of intraluminal contact mediated guidance signals on axonal mismatch during peripheral nerve repair. Biomaterials 2012;33:6660−71.
[20] Leclerc E, Furukawa KS, Miyata F, Sakai Y, Ushida T, Fujii T. Fabrication of microstructures in photosensitive biodegradable polymers for tissue engineering applications. Biomaterials 2004;25:4683−90.
[21] Harding AJ, Christmas CR, Ferguson MW, Loescher AR, Robinson PP, Boissonade FM. Mannose-6-phosphate facilitates early peripheral nerve regeneration in thy-1-YFP-H mice. Neuroscience 2014;279:23−32.
[22] Ortega Í Deshpande P, Gill AA, Macneil S, Claeyssens F. Development of a microfabricated artificial limbus with micropockets for cell delivery to the cornea. Biofabrication 2013;5:025008.
[23] Johnson DW, Sherborne C, Didsbury MP, Pateman C, Cameron NR, Claeyssens F. Macrostructuring of emulsion-templated porous polymers by 3D laser patterning. Adv Mater 2013;25:3178−81.
[24] Koroleva A, Gill AA, Ortega I, Haycock JW, Schlie S, Gittard SD, et al. Two-photon polymerization-generated and micromolding-replicated 3D scaffolds for peripheral neural tissue engineering applications. Biofabrication 2012;4:025005.
[25] Melissinaki V, Gill AA, Ortega I, Vamvakaki M, Ranella A, Haycock JW, et al. Direct laser writing of 3D scaffolds for neural tissue engineering applications. Biofabrication 2011;3:045005.
[26] Arcaute K, Mann BK, Wicker RB. Fabrication of off-the-shelf multilumen poly(ethylene glycol) nerve guidance conduits using stereolithography. Tissue Eng Part C Methods 2010;17(1):27−38.
[27] Arcaute K, Mann BK, Wicker RB. Stereolithography of three-dimensional bioactive poly(ethylene glycol) constructs with encapsulated cells. Ann Biomed Eng 2006;34:1429−41.
[28] Beke S, Farkas B, Romano I, Brandi F. 3D scaffold fabrication by mask projection excimer laser stereolithography. Opt Mater Express 2014;4(10):2032−41.
[29] Aberg M, Ljungberg C, Edin E, Millqvist H, Nordh E, Theorin A, et al. Clinical evaluation of a resorbable wrap-around implant as an alternative to nerve repair: a prospective, assessor-blinded, randomised clinical study of sensory, motor and functional recovery after peripheral nerve repair. J Plast Reconstr Aesthet Surg 2009;62:1503−9.
[30] Armstrong SJ, Wiberg M, Terenghi G, Kingham PJ. ECM molecules mediate both Schwann cell proliferation and activation to enhance neurite outgrowth. Tissue Eng 2007;13:2863−70.
[31] Murray-Dunning C, McArthur SL, Sun T, McKean R, Ryan AJ, Haycock JW. Three-dimensional alignment of Schwann cells using hydrolysable microfiber scaffolds: strategies for peripheral nerve repair. Methods Mol Biol 2011;695: 155−16.
[32] Buttiglione M, Vitiello F, Sardella E, Petrone L, Nardulli M, Favia P, et al. Behaviour of SH-SY5Y neuroblastoma cell line grown in different media and on different chemically modified substrates. Biomaterials 2007;28:2932−45.
[33] Thornton MR, Shawcross SG, Mantovani C, Kingham PJ, Birchall MA, Terenghi G. Neurotrophins 3 and 4 differentially regulate NCAM, L1 and N-cadherin expression during peripheral nerve regeneration. Biotechnol Appl Biochem 2008;49:165−74.
[34] Wilson ADH, Hart A, Wiberg M, Terenghi G. Acetyl-L-carnitine increases nerve regeneration and target organ reinnervation − a morphological study. J Plast Reconstr Aesthet Surg 2010;63:1186−95.
[35] Yao L, de Ruiter GC, Wang H, Knight AM, Spinner RJ, Yaszemski MJ, et al. Controlling dispersion of axonal regeneration using a multichannel collagen nerve conduit. Biomaterials 2010;31:5789−97.
[36] Kim YT, Haftel VK, Kumar S, Bellamkonda RV. The role of aligned polymer fiber-based constructs in the bridging of long peripheral nerve gaps. Biomaterials 2008;29:3117−27.

[37] Jha BS, Colello RJ, Bowman JR, Sell SA, Lee KD, Bigbee JW, et al. Two pole air gap electrospinning: fabrication of highly aligned, three-dimensional scaffolds for nerve reconstruction. Acta Biomater 2011;7:203—15.

[38] Daud MF, Pawar KC, Claeyssens F, Ryan AJ, Haycock JW. An aligned 3D neuronal-glial co-culture model for peripheral nerve studies. Biomaterials 2012;33:5901—13.

[39] Mosahebi A, Woodward B, Wiberg M, Martin R, Terenghi G. Retroviral labeling of Schwann cells: in vitro characterization and in vivo transplantation to improve peripheral nerve regeneration. Glia 2001;34:8—17.

[40] Mosahebi A, Fuller P, Wiberg M, Terenghi G. Effect of allogeneic Schwann cell transplantation on peripheral nerve regeneration. Exp Neurol 2002;173: 213—23.

[41] Caddick J, Kingham PJ, Gardiner NJ, Wiberg M, Terenghi G. Phenotypic and functional characteristics of mesenchymal stem cells differentiated along a Schwann cell lineage. Glia 2006;54:840—9.

[42] di Summa PG, Kalbermatten DF, Pralong E, Raffoul W, Kingham PJ, Terenghi G. Long-term in vivo regeneration of peripheral nerves through bioengineered nerve grafts. Neuroscience 2011;181:278—91.

[43] di Summa PG, Kingham PJ, Raffoul W, Wiberg M, Terenghi G, Kalbermatten DF. Adipose-derived stem cells enhance peripheral nerve regeneration. J Plast Reconstr Aes 2010;63:1544—52.

[44] Erba P, Mantovani C, Kalbermatten DF, Pierer G, Terenghi G, Kingham PJ. Regeneration potential and survival of transplanted undifferentiated adipose tissue-derived stem cells in peripheral nerve conduits. J Plast Reconstr Aes 2010;63:E811—7.

[45] Kingham PJ, Kalbermatten DF, Mahay D, Armstrong SJ, Wiberg M, Terenghi G. Adipose-derived stem cells differentiate into a Schwann cell phenotype and promote neurite outgrowth in vitro. Exp Neurol 2007;207(2):267—74.

[46] Xu QG, Midha R, Martinez JA, Glio G, Zochodne DW. Facilitated sprouting in a peripheral nerve injury. Neuroscience 2008;152:877—87.

[47] Arcaute K, Mann B, Wicker R. Stereolithography of spatially controlled multi-material bioactive poly(ethylene glycol) scaffolds. Acta Biomater 2010;6: 1047—54.

[48] Charles PT, Stubbs VR, Soto CM, Martin BD, White BJ, Taitt CR. Reduction of non-specific protein adsorption using poly(ethylene) glycol (PEG) modified polyacrylate hydrogels in immunoassays for staphylococcal enterotoxin B detection. Sensors (Basel) 2009;9:645—55.

[49] Sofia SJ, Premnath V, Merrill EW. Poly(ethylene oxide) grafted to silicon surfaces: grafting density and protein adsorption. Macromolecules 1998;31: 5059—70.

[50] Ovsianikov A, Malinauskas M, Schlie S, Chichkov B, Gittard S, Narayan R, et al. Three-dimensional laser micro- and nano-structuring of acrylated poly(-ethylene glycol) materials and evaluation of their cytoxicity for tissue engineering applications. Acta Biomat 2011;7:967—74.

[51] Aimetti AA, Tibbitt MW, Anseth KS. Human neutrophil elastase responsive delivery from poly(ethylene glycol) hydrogels. Biomacromol 2009;10: 1484—9.

[52] Mahoney MJ, Anseth KS. Three-dimensional growth and function of neural tissue in degradable polyethylene glycol hydrogels. Biomaterials 2006;27: 2265—74.

[53] Zhu J. Bioactive modification of poly (ethylene glycol) hydrogels for tissue engineering. Biomaterials 2010;31:4639—56.

[54] Quellec P, Gref R, Perrin L, Dellacherie E, Sommer F, Verbavatz JM, et al. Protein encapsulation within polyethylene glycol-coated nanospheres. I. Physicochemical characterization. J Biomed Mater Res 1998;42:45—54.

[55] Mitchel JA, Hoffman-Kim D. Cellular scale anisotropic topography guides Schwann cell motility. PLoS One 2011;6:e24316.

[56] Menovsky T, Beek JF. Laser, fibrin glue, or suture repair of peripheral nerves: a comparative functional, histological, and morphometric study in the rat sciatic nerve. J Neurosurg 2001;95:694—9.

[57] Ngeow WC, Atkins S, Morgan CR, Metcalfe AD, Boissonade FM, Loescher AR, et al. The effect of mannose-6-phosphate on recovery after sciatic nerve repair. Brain Res 2011;1394:40—8.

[58] Borschel GH, Kia KF, Kuzon Jr WM, Dennis RG. Mechanical properties of acellular peripheral nerve. J Surg Res 2003;114:133—9.